View metadata, citation and similar papers at core.ac.uk
brought to you by CORE
provided by Helsingin yliopiston digitaalinen arkisto

Numerical comparison of spectral properties of volume-integral-equation formulations

Johannes Markkanen[a,*], Pasi Ylä-Oijala[b]

[a]Department of Physics, PO Box 64, FI-00014, University of Helsinki, Finland
[b]Department of Radio Science and Engineering,P.O. Box 13000, FI-00076, Aalto University, Finland

Abstract

We study and compare spectral properties of various volume-integral-equation formulations. The equations are written for the electric flux, current, field, and potentials, and discretized with basis functions spanning the appropriate function spaces. Each formulation leads to eigenvalue distributions of different kind due to the effects of discretization procedure, namely, the choice of basis and testing functions. The discrete spectrum of the potential formulation reproduces the theoretically predicted spectrum almost exactly while the spectra of other formulations deviate from the ideal one. It is shown that the potential formulation has the spectral properties desired from the preconditioning perspective.

Keywords: spectrum of integral operator, numerical modeling, volume-integral-equation

1. Introduction

Electromagnetic scattering problems involving inhomogeneous objects are often solved by the volume-integral-equation methods (VIE). The VIE method is suitable for complicated scattering problems due to its simplicity; only the Green's function of the background is required. Moreover, the radiation condition is automatically satisfied. The drawback in the VIEs is that the discretization procedure leads to a full matrix equation in contrast to, for example, the finite-element method where the system is sparse. This implies that to obtain a solution for the matrix equation is of order $O(N^3)$ complexity for time and $O(N^2)$ for memory, where N is the number of unknowns. For the lowest order basis, typically 10 unknowns per wavelength are needed.

High computational complexity prevents the usage of the direct VIE solvers for large structures. Using an iterative method such as the conjugate-gradient (CG) or generalized minimal residual (GMRES) method, the solution time is reduced to $O(MN^2)$ where M is the number of iterations needed to solve the system. By accelerating the matrix-vector multiplication required in each iteration step with, e.g., a fast multilevel multipole algorithm (MLFMA) or fast Fourier transform (FFT) based techniques [1, 2, 3, 4, 5], the computational complexity is reduced to $O(MNlogN)$ for time and $O(N) - O(NlogN)$ for memory. Hence, solution time becomes manageable if $M << N$.

For an efficient algorithm it is necessary that the number of iterations M is much smaller than N. M depends on the conditioning of the matrix which, in turn, depends on materials, size, and shape of the scatterer. Unfortunately, the number of iterations increases rapidly with respect to the permittivity and size [6, 7, 8, 9]. To understand reasons for this, we need to study the spectrum of the integral operator. Theoretically, the spectrum of the volume integral operator has been studied in [10, 11, 12]. These studies show that the spectrum and the spectral radius depend on the permittivity function. The spectral radius, in turn, defines the conditioning of the matrix, and consequently, the convergence of the iterative solution.

The spectral properties of the discrete system (the eigenvalues of the matrix) depend on the discretization technique employed, hence, it is important to study the effects of discretization numerically. Numerical studies, however, have been restricted to a couple of the most popular volume-integral-equation formulations and discretizations. The discrete-dipole-approximation (DDA) type formulations with cubic elements were analyzed in [10, 13, 14], and with rectangular elements in [15]. Moreover, the spectral properties of the electric current J-VIE with the L^2 Galerkin dicretization for tetrahedral mesh have been studied [16]. It is worth noting that the integration of Green's tensor (IGT) formulation of the DDA is almost equivalent to the J-VIE discretized with cubic elements and point matching. The only difference is that the DDA maps the polarization current to the electric field and the J-VIE maps the current to itself, hence, the matrix elements differ by a factor of $(\epsilon_r - 1)$.

In this paper, we compare the eigenvalue distributions computed by four VIE formulations and their standard discretizations. We consider the electric flux density formulation (D-VIE) discretized with the SWG (Schaubert-Wilton-Glisson) basis and testing functions [17], field formulation (E-VIE) with the curl conforming basis and testing functions [18, 19], current formulation (J-VIE) [20] with L^2 basis and testing functions, and potential formulation (P-VIE) with scalar and vector H^1 basis function and point matching [21]. We apply linear linear tetrahedral elements for discretizations and the results presented here cannot be directly generalized to other element shapes such as rectangular or curvilinear elements.

*Corresponding author. Tel.: +358504160605.
E-mail address: johannes.markkanen@helsinki.fi

2. Formulations

Consider time-harmonic electromagnetic wave scattering by an inhomogeneous dielectric object bounded by volume V in free space. The time factor of $exp(-i\omega t)$ is assumed and suppressed. The relative permittivity $\epsilon_r(\boldsymbol{r})$ may be a function of position in V. The background is homogeneous with constant ϵ_0 and μ_0. Let us define the volume potential operator as

$$\mathcal{V}(\boldsymbol{F})(\boldsymbol{r}) = \int_V G(\boldsymbol{r},\boldsymbol{r}')\,\boldsymbol{F}(\boldsymbol{r}')\,dV', \tag{1}$$

where G is the Green's function of the background. By using the volume-equivalence principle, the following representations are obtained for the total electric $\boldsymbol{E}$, and magnetic $\boldsymbol{H}$ fields [22]

$$\begin{aligned} \boldsymbol{E} &= \boldsymbol{E}^{inc} + \frac{-1}{i\omega\epsilon_0}(\nabla\nabla + k^2\bar{\bar{I}})\cdot\mathcal{V}(\boldsymbol{J}) - \nabla\times\mathcal{V}(\boldsymbol{M}) \\ \boldsymbol{H} &= \boldsymbol{H}^{inc} + \frac{-1}{i\omega\mu_0}(\nabla\nabla + k^2\bar{\bar{I}})\cdot\mathcal{V}(\boldsymbol{M}) + \nabla\times\mathcal{V}(\boldsymbol{J}) \end{aligned} \tag{2}$$

in which $\boldsymbol{E}^{\text{inc}}$ and $\boldsymbol{H}^{\text{inc}}$ denote the incident fields with sources outside the object. The source functions in (2) are the equivalent electric and magnetic current densities

$$\begin{aligned} \boldsymbol{J}(\boldsymbol{r}) &= -i\omega\epsilon_0(\epsilon_r(\boldsymbol{r})-1)\boldsymbol{E}(\boldsymbol{r}) \\ \boldsymbol{M}(\boldsymbol{r}) &= -i\omega\mu_0(\mu_r(\boldsymbol{r})-1)\boldsymbol{H}(\boldsymbol{r}). \end{aligned} \tag{3}$$

From now on we assume that the permeability $\mu_r = 1$, hence the magnetic current $\boldsymbol{M}$ is identically zero. Based on the representations in (2), we can derive three VIE formulations. The most widely used formulation is the D-formulation or D-VIE in which the unknown function is the flux density $\boldsymbol{D}$ [17, 23]. By representing the equivalent current $\boldsymbol{J}$ in terms of the flux density and inserting it into (2), the D-VIE is obtained:

$$\epsilon_0\boldsymbol{E}^{\text{inc}} = \bar{\bar{\epsilon}}_r^{-1}\cdot\boldsymbol{D} - (\nabla\nabla + k^2\bar{\bar{I}})\cdot\mathcal{V}(\bar{\bar{\chi}}\cdot\boldsymbol{D}). \tag{4}$$

Here the material parameter $\bar{\bar{\chi}} = \bar{\bar{I}} - \bar{\bar{\epsilon}}_r^{-1}$.

The integral-equation can be written for the equivalent polarization current $\boldsymbol{J}$ which is the actual source for the scattered fields [20]. We call this formulation as the J-formulation or J-VIE, and it reads as

$$\boldsymbol{J}^{\text{inc}} = \boldsymbol{J} - \bar{\bar{\tau}}\cdot(\nabla\nabla + k^2\bar{\bar{I}})\cdot\mathcal{V}(\boldsymbol{J}), \tag{5}$$

where $\bar{\bar{\tau}} = \bar{\bar{\epsilon}}_r - \bar{\bar{I}}$.

To derive the electric field E-formulation (E-VIE), we use the identity

$$(\nabla\nabla + k^2\bar{\bar{I}})\cdot\mathcal{V}(\boldsymbol{F}) = \nabla\times(\nabla\times\mathcal{V}(\boldsymbol{F})) - \boldsymbol{F}, \tag{6}$$

since it is more natural to apply the curl rather than div-operator to the electric field. Representing the unknown in terms of the electric field, the E-VIE can be written as follows: [19, 18]:

$$\boldsymbol{E}^{\text{inc}} = \bar{\bar{\epsilon}}_r\cdot\boldsymbol{E} - \nabla\times\nabla\times\mathcal{V}(\bar{\bar{\tau}}\cdot\boldsymbol{E}). \tag{7}$$

Finally, the integral-equation for the vector $\boldsymbol{A}$ and scalar ϕ potentials, defined as

$$\boldsymbol{E} = i\omega\boldsymbol{A} - \nabla\phi, \quad \boldsymbol{H} = \mu_0^{-1}\nabla\times\boldsymbol{A}, \tag{8}$$

can be derived by applying the Lorentz gauge

$$i\omega\nabla\cdot\boldsymbol{A} = -k^2\phi \tag{9}$$

in which case both potentials satisfy the Helmholtz equation. Using the volume-equivalence principle, the potential formulation P-VIE can be written as [24]

$$\begin{cases} i\omega\boldsymbol{A}^{inc} &= i\omega\boldsymbol{A} - k^2\mathcal{V}[\bar{\bar{\tau}}\cdot(i\omega\boldsymbol{A} - \nabla\phi)] \\ \phi^{inc} &= \phi - \mathcal{S}[\bar{\bar{\tau}}\cdot(i\omega\boldsymbol{A} - \nabla\phi)] \end{cases} \tag{10}$$

in which

$$\mathcal{S}(\boldsymbol{F})(\boldsymbol{r}) = \int_S \boldsymbol{n}(\boldsymbol{r}')\cdot\boldsymbol{F}(\boldsymbol{r}')G(\boldsymbol{r},\boldsymbol{r}')\,\mathrm{d}S', \tag{11}$$

and $\boldsymbol{n}'$ is the outer unit normal vector of the surfaces S on which the permittivity is discontinuous.

3. Discretizations

In this section, we consider discretizations of the D-, J-, E-, and P-formulations. Let us divide the object with linear tetrahedral elements, and define the basis $\boldsymbol{b}$ and the testing $\boldsymbol{t}$ functions on the tetrahedral mesh. The residual error is forced to be orthogonal to test functions with the symmetric L^2 product.

$$\langle\boldsymbol{F},\boldsymbol{G}\rangle = \int_V \boldsymbol{F}\cdot\boldsymbol{G}\,\mathrm{d}V, \tag{12}$$

where V is the volume of the object.

As pointed out in [25] and [26] to guarantee the convergence in the norm of the solution, testing functions should span the L^2 dual space of the range of the integral operator. The mapping properties of the formulations read as

$$\begin{array}{rcl} \text{D-formulation:} & H_{div}(\Omega)^3 & \rightarrow \quad H_{curl}(\Omega)^3 \\ \text{E-formulation:} & H_{curl}(\Omega)^3 & \rightarrow \quad H_{div}(\Omega)^3 \\ \text{J-formulation:} & L^2(\Omega)^3 & \rightarrow \quad L^2(\Omega)^3 \\ \text{P-formulation:} & H^1(\Omega)^3\times H^1(\Omega)^1 & \rightarrow \quad H^1(\Omega)^3\times H^1(\Omega)^1, \end{array}$$

where L^2 is a function space of square integrable functions, and

$$\begin{aligned} H_{div}(\Omega)^3 &= \{\boldsymbol{f}\,|\,\boldsymbol{f}\in L^2(\Omega)^3 \wedge \nabla\cdot\boldsymbol{f}\in L^2(\Omega)^1\} \\ H_{curl}(\Omega)^3 &= \{\boldsymbol{f}\,|\,\boldsymbol{f}\in L^2(\Omega)^3 \wedge \nabla\times\boldsymbol{f}\in L^2(\Omega)^3\} \\ H^1(\Omega)^1 &= \{f\,|\,f\in L^2(\Omega)^1 \wedge \nabla f\in L^2(\Omega)^3\} \end{aligned} \tag{13}$$

and $H^1(\Omega)^3$ is a function space of 3D-vectors whose components are in $H^1(\Omega)^1$.

We apply Galerkin's method with identical basis and testing functions to discretize the J-, D-, and E-formulations. Since H_{div} and H_{curl} are L^2 dual to each other and L^2 is dual to itself, we can see that the J-, D-, and E-equations are tested in

the dual space of the range when Galerkin's testing is applied. Galerkin's testing may not work for the P-formulations since the L^2 dual space of H^1 is H^{-1}. We use the point-matching scheme since it has been used earlier in [21]. It should be noted, however, that Knonecker's delta functions, i.e., test functions in the point-matching procedure, do not span the proper dual space of H^1 which may lead to accuracy problems.

3.1. Discretization of D-formulation

The D-formulation is discretized with Galerkin's method using the lowest mixed order divergence conforming SWG basis $\boldsymbol{b}^{div}$ and testing functions $\boldsymbol{t}^{div}$ [17] which span the finite-dimensional H_{div} space. The SWG function associated to the face having nodes ijk is defined in terms of the nodal function N_i as

$$\boldsymbol{b}^{div}_{ijk} = 2A_{ijk}[N_i(\nabla N_j \times \nabla N_k) + N_j(\nabla N_k \times \nabla N_i) + N_k(\nabla N_i \times \nabla N_j)] \tag{14}$$

where A_{ijk} is the area of face ijk. The hyper-singularity of the kernel is reduced by moving one derivative into the testing function and another into the basis function by integrating by parts. Since basis and testing functions are divergence conforming, some of the surface integrals cancel out on element boundaries. The elements of the system matrix can be written as

$$\begin{aligned}
A^D_{mn} &= \left\langle \boldsymbol{t}^{\mathrm{div}}_m,\, \bar{\bar{\epsilon}}^{-1}_m \cdot \boldsymbol{b}^{div}_n - \left(\nabla\nabla\cdot + k^2\right)\boldsymbol{\mathcal{S}}(\bar{\bar{\chi}}_n \cdot \boldsymbol{b}^{\mathrm{div}}_n)\right\rangle_{V_m} \\
&= \int_{V_m} \boldsymbol{t}^{div}_m \cdot (\bar{\bar{\epsilon}}^{-1}_m \cdot \boldsymbol{b}^{div}_n)\,\mathrm{d}V \\
&+ \int_{\partial V_m} \boldsymbol{n}\cdot\boldsymbol{t}^{div}_m \int_{\partial V_n} G\,\boldsymbol{n}'\cdot(\bar{\bar{\chi}}_n\cdot\boldsymbol{b}^{div}_n)\,\mathrm{d}S'\,\mathrm{d}S \\
&+ \int_{V_m} (\nabla\cdot\boldsymbol{t}^{div}_m)\int_{V_n} G\,\nabla'\cdot(\bar{\bar{\chi}}_n\cdot\boldsymbol{b}^{div}_n)\,\mathrm{d}V'\,\mathrm{d}V \\
&- \int_{V_m} (\nabla\cdot\boldsymbol{t}^{div}_m)\int_{\partial V_n} G\,\boldsymbol{n}'\cdot(\bar{\bar{\chi}}_n\cdot\boldsymbol{b}^{div}_n)\,\mathrm{d}S'\,\mathrm{d}V \\
&- \int_{\partial V_m} \boldsymbol{n}\cdot\boldsymbol{t}^{div}_m \int_{V_n} G\,\nabla'\cdot(\bar{\bar{\chi}}_n\cdot\boldsymbol{b}^{div}_n)\,\mathrm{d}V'\,\mathrm{d}S \\
&- \int_{V_m} \boldsymbol{t}^{div}_m\cdot k^2\bar{\bar{I}}\cdot\int_{V_n} G(\bar{\bar{\chi}}_n\cdot\boldsymbol{b}^{div}_n)\,\mathrm{d}V'\mathrm{d}V.
\end{aligned} \tag{15}$$

3.2. Discretization of E-formulation

The unknown electric $\boldsymbol{E}$ field has continuous tangential components on element boundaries, hence the field should be expanded with curl conforming basis functions (H_{curl}). In terms of the nodal functions, the curl conforming function associated to the edge e_{ij} is expressed as

$$\boldsymbol{b}^{curl}_{ij} = l_{ij}(N_i\nabla N_j - N_j\nabla N_i), \tag{16}$$

in which l_{ij} is the length of the edge e_{ij}. Analogously to the case of the D-formulation, we can discretize the operator of the E-formulation with the curl conforming basis $\boldsymbol{b}^{curl}$ and testing $\boldsymbol{t}^{curl}$ functions as

$$\begin{aligned}
A^E_{mn} &= \left\langle \boldsymbol{t}^{\mathrm{curl}}_m,\, \bar{\bar{\epsilon}}_m\cdot\boldsymbol{b}^{curl}_n - \nabla\times\nabla\times\boldsymbol{\mathcal{S}}(\bar{\bar{\tau}}_n\cdot\boldsymbol{b}^{\mathrm{curl}}_n)\right\rangle_V \\
&= \int_{V_m} \boldsymbol{t}^{curl}_m\cdot(\bar{\bar{\epsilon}}_m\cdot\boldsymbol{b}^{curl}_n)\,\mathrm{d}V \\
&+ \int_{\partial V_m} \boldsymbol{n}\times\boldsymbol{t}^{curl}_m\cdot\int_{\partial V_n} G\,\boldsymbol{n}'\times(\bar{\bar{\tau}}_n\cdot\boldsymbol{b}^{curl}_n)\,\mathrm{d}S'\,\mathrm{d}S \\
&+ \int_{V_m} (\nabla\times\boldsymbol{t}^{curl}_m)\int_{V_n} G\,\nabla'\times(\bar{\bar{\tau}}_n\cdot\boldsymbol{b}^{curl}_n)\,\mathrm{d}V'\,\mathrm{d}V \\
&- \int_{V_m} (\nabla\times\boldsymbol{t}^{curl}_m)\int_{\partial V_n} G\,\boldsymbol{n}'\times(\bar{\bar{\tau}}_n\cdot\boldsymbol{b}^{curl}_n)\,\mathrm{d}S'\,\mathrm{d}V \\
&- \int_{\partial V_m} \boldsymbol{n}\times\boldsymbol{t}^{curl}_m\int_{V_n} G\,\nabla'\times(\bar{\bar{\tau}}_n\cdot\boldsymbol{b}^{curl}_n)\,\mathrm{d}V'\,\mathrm{d}S.
\end{aligned} \tag{17}$$

3.3. Discretization of J-formulation

The equivalent volume currents have no continuities across interfaces of discontinuous permittivity. Hence, it is essential that basis functions $\boldsymbol{b}^L$ do not enforce any continuity across the element interfaces. We use piecewise constant basis and testing functions to expand the unknowns (three functions in each tetrahedra). These functions can be written as

$$\boldsymbol{b}^L_{ijkl} = \frac{1}{\sqrt{V_{ikjl}}}(N_i + N_j + N_k + N_l)\hat{\boldsymbol{e}}_{xyz} = \frac{1}{\sqrt{V_{ikjl}}}\hat{\boldsymbol{e}}_{xyz}, \tag{18}$$

in which $\hat{\boldsymbol{e}}_{xyz}$ corresponds unit vector $\hat{\boldsymbol{e}}_x$ or $\hat{\boldsymbol{e}}_y$ or $\hat{\boldsymbol{e}}_z$, and V_{ijkl} is the volume of element $ijkl$. By moving one derivative into the testing function and the other into the basis function, we obtain

$$\begin{aligned}
A^J_{mn} &= \left\langle \boldsymbol{t}^L_m,\, \boldsymbol{b}^L_n - \bar{\bar{\tau}}_m\cdot(\nabla\nabla + k^2\bar{\bar{I}})\cdot\boldsymbol{\mathcal{S}}(\boldsymbol{b}^L_n)\right\rangle_{V_m} \\
&= \int_{V_m} \boldsymbol{t}^L_m\cdot\boldsymbol{b}^L_n\,\mathrm{d}V \\
&+ \int_{\partial V_m} \boldsymbol{n}\cdot(\bar{\bar{\tau}}^T_m\cdot\boldsymbol{t}^L_m)\cdot\int_{\partial V_n} G\,\boldsymbol{n}'\cdot\boldsymbol{b}^L_n\,\mathrm{d}S'\,\mathrm{d}S \\
&- \int_{V_m} \boldsymbol{t}^L_m\cdot\bar{\bar{\tau}}_m\cdot k^2\bar{\bar{I}}\cdot\int_{V_n} G\boldsymbol{b}^L_n\,\mathrm{d}V'\mathrm{d}V,
\end{aligned} \tag{19}$$

where $\bar{\bar{\tau}}^T$ denotes the transpose of $\bar{\bar{\tau}}$.

3.4. Discretization of P-formulation

In the potential formulation, we have two different unknowns and two equations for the vector and scalar potentials. The scalar potential is expanded by the standard nodal basis functions N^{H1}_n, and each component of the vector potential is represented by the nodal basis function giving a vector H^1-function $\boldsymbol{N}^{H1}_n$.

The point-matching scheme is applied to discretize the equations, i.e., test functions are Knonecker's delta functions δ_m at nodes. Hence, we can write the system matrix as a block matrix

$$A^P = \begin{pmatrix} A_xA_x & A_xA_y & A_xA_z & A_xV \\ A_yA_x & A_yA_y & A_yA_z & A_yV \\ A_zA_x & A_zA_y & A_zA_z & A_zV \\ VA_x & VA_y & VA_z & VV \end{pmatrix} \tag{20}$$

where

$$
\begin{aligned}
(A_iA_j)_{mn} &= \hat{\boldsymbol{e}}_i \cdot \hat{\boldsymbol{e}}_j \delta_m N_m - \hat{\boldsymbol{e}}_i \cdot k^2 \int_{V_n} (\bar{\bar{\tau}}_n \cdot \hat{\boldsymbol{e}}_j) N_n G \, \mathrm{d}V' \\
(A_iV)_{mn} &= \hat{\boldsymbol{e}}_i \cdot k^2 \int_{V_n} (\bar{\bar{\tau}}_n \cdot \nabla' N_n) G \, \mathrm{d}V' \\
(VA_j)_{mn} &= -\int_{\partial V_n} \boldsymbol{n}' \cdot (\bar{\bar{\tau}}_n \cdot \hat{\boldsymbol{e}}_j N_n) G \, \mathrm{d}S' \\
(VV)_{mn} &= \delta_m N_m + \int_{\partial V_n} \boldsymbol{n}' \cdot (\bar{\bar{\tau}}_n \cdot \nabla' N_n) G \, \mathrm{d}S'.
\end{aligned}
\tag{21}
$$

4. Numerical experiments

In this section, we study numerical properties of the formulations and discretizations developed in the previous section. We consider numerical spectra and accuracy of the discretized systems and briefly discuss preconditioning strategies based on the spectral properties.

4.1. Numerical spectra

First, we consider a small spherical object discretized with 676 tetrahedral elements. The size parameter of the sphere $kr = 0.01$ and the relative permittivity $\epsilon_r = 5$. The object is small compared to the wavelength since we are interested in the essential spectrum. At higher frequencies, discrete eigenvalues associated with resonance solutions appear [10]. Fig. 1 shows the eigenvalues of the discretized matrices arising from the J-, D-, E-, and P-formulations (blue stars), and the red circles denote theoretically predicted accumulation points of eigenvalues when the scatterer is a smooth sphere [12]. Three accumulation points are predicted for an object with smooth surface and the essential spectrum $\sigma_e = \{1, \frac{\epsilon_r+1}{2}, \epsilon_r\}$. For objects with non-smooth surfaces, the spectrum is bounded between 1 and ϵ_r.

From Fig. 1 it is evident that some eigenvalues of the D- and E-formulations locate outside the bounds 1 and ϵ_r whereas the eigenvalues of the J- and P- formulations lie between the bounds. The reason that the D-, and E-formulations behave such a way is that the basis and test functions do not form an orthogonal dual pair, i.e., the Gram matrices $< \boldsymbol{t}_m^{div}, \boldsymbol{b}_n^{div} >$ and $< \boldsymbol{t}_m^{curl}, \boldsymbol{b}_n^{curl} >$ are not the identity matrices. It is possible to cancel this effect by multiplying the operator by the inverse of the Gram matrix. This is demonstrated in Fig. 2. Now all the spectra lie in a line segment between points 1 and ϵ_r. It should be noted here that multiplying the J- or P-formulations with the inverse of the Gram matrix does not affect the spectrum since in these formulations the Gram matrix is the identity matrix.

4.2. Dimensions of subspaces

Let us recall the (incomplete) Helmholtz decomposition of involved function spaces:

$$
\begin{aligned}
L^2(\Omega) &= \nabla H_0^1(\Omega) + \nabla \times H_{curl,0}(\Omega) + \boldsymbol{W}(\Omega) \\
H_{div}(\Omega) &= \nabla \times H_{curl,0}(\Omega) + X_{nsol}(\Omega) \\
H_{curl}(\Omega) &= \nabla H_0^1(\Omega) + X_{nirr}(\Omega),
\end{aligned}
\tag{22}
$$

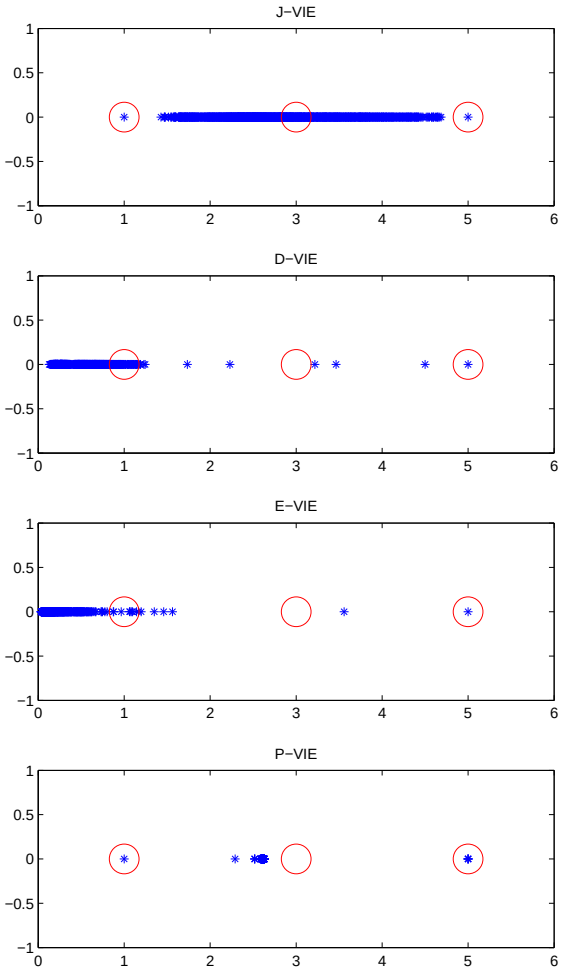

Figure 1: Eigenvalues of the J-VIE, D-VIE, E-VIE, and P-VIE matrices (blue stars). Theoretically expected accumulation points of eigenvalues in case of a smooth surface (red circles). The scatterer is a dielectric ($\epsilon_r = 5$) sphere of size $kr = 0.01$ discretized by 676 tetrahedral elements.

in which $\boldsymbol{W}$ denotes the gradients of harmonic H^1 fields, X_{nsol} is the space of non-solenoidal H_{div} functions, and X_{nirr} is the space of non-irrotational H_{curl} functions. The subscript 0 in H_0 denotes vanishing boundary value, and vanishing tangential trace in $H_{curl,0}$.

Now, we can investigate dimensions of the above-mentioned subspaces. Fig. 3 shows the real part of the eigenvalue with respect to the spectral index. Here, we note that each formulation leads to a different number of unknowns, hence the number of eigenvalues is not the same for all formulations. The J-VIE gives $3N_t$, D-VIE N_f, E-VIE N_e, and P-VIE $4N_n$ unknowns and eigenvalues, where N_t, N_f, N_e, and N_n are the number of tetrahedra, faces, edges, and nodes, respectively. In Table 1, the number of tetrahedra, nodes, edges, and faces in the applied tetrahedral mesh are presented. In addition, the number

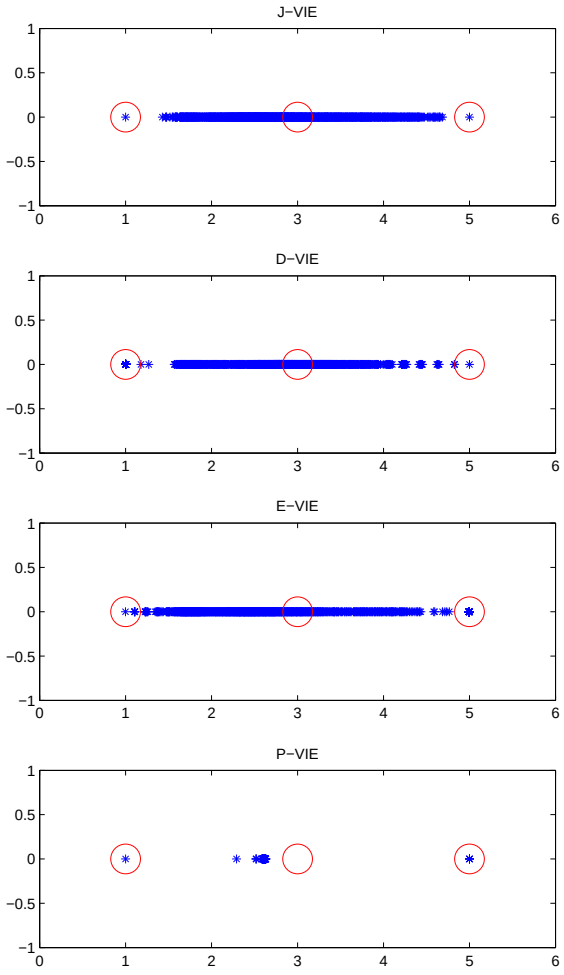

Figure 2: Same as in Fig. 1 except the system matrices are multiplied by the inverses of associated Gram matrices.

of boundary and interior nodes, edges, and faces are shown.

For the J-VIE formulation, we find that there are 577 eigenvalues at 1. As discussed in [16], the solenoidal ($\nabla\times H_{curl,0}$) subspace of L^2 is responsible of eigenvalues at 1. The solenoidal subspace of the space spanned by the piecewise constant functions is associated with the interior edges ($\nabla \times \boldsymbol{b}^{curl}$) and the degrees of freedom is $dof = N_e^i - N_n^i = 577$ where N_e^i, N_n^i are the number of interior edges and nodes, respectively. The same solenoidal subspace is part of the space spanned by the SWG-functions used in the D-formulation [23], and therefore, we can find 577 eigenvalues at 1.

The other accumulation point at $\epsilon_r = 5$ is due to the irrotational (∇H_0^1) subspace [16]. Irrotational subspace can be spanned by the ∇N_i functions associated to the interior nodes of the mesh. Hence, we can detect 70 eigenvalues at 5 in case of the J-, and E-formulations.

In the J-VIE, the remaining eigenvalues are due to the gradients of the harmonic H^1-functions with $N_f - N_n^i$ degrees of freedom. This space corresponds equivalent surface charges on element boundaries. The remaining eigenvalues of the D-VIE are related to the non-solenoidal part (X_{nsol}) of the flux density with $N_t + N_e^b - N_n^b$ degrees of freedom. The non-irrotational part (X_{nirr}) of the field in the E-VIE has $N_f - N_t + N_n^b$ degrees of freedom.

Table 1: Details of the mesh.

	total	interior	boundary
tetrahedra	676	-	-
nodes	172	70	102
edges	947	647	300
faces	1452	1252	200

In the P-VIE, we can directly observe that the equation for the vector potential is of the form identity + compact in $H^1(\Omega)^3$, hence all the eigenvalues ($3N_n$) accumulate to 1. Let us take a look at the scalar potential equation

$$\begin{aligned} \phi^{inc} &= \phi - \int_S \boldsymbol{n}' \cdot (\epsilon_r - 1)(i\omega\boldsymbol{A} - \nabla'\phi) G \, \mathrm{d}S' \\ &= \phi - \int_S \boldsymbol{n}' \cdot (\epsilon_r - 1)(i\omega\boldsymbol{A}) G \, \mathrm{d}S' \\ &+ p.v. \int_S (\epsilon_r - 1)\partial_{n'} G\phi \, \mathrm{d}S' \\ &+ \frac{\Omega_r}{4\pi}(\epsilon_r - 1)\phi, \end{aligned} \tag{23}$$

where, $\partial_{n'}G$ denotes the normal derivative of the Green's functions with respect to $\boldsymbol{r}'$, and Ω_r is the solid angle the test point $\boldsymbol{r}$ sees the domain enclosed by surface S. If $\boldsymbol{r}$ is inside the object $\Omega_r = 4\pi$, and if $\boldsymbol{r}$ lies on the smooth surface $\Omega_r = 2\pi$, and $\Omega_r = 0$ when $\boldsymbol{r}$ is outside the object. The spectrum of the operator can be easily found because the first integral in (23) is a compact operator, and the second integral is compact on smooth surfaces (bounded on non-smooth surfaces).

Since we have N_n^i test points inside the object, N_n^i eigenvalues are accumulated at 5, and on the surface we have N_n^b test points, giving N_n^b eigenvalues around $(\epsilon_r + 1)/2 = 3$. The eigenvalues are slightly shifted towards 1 because the solid angle seen by the boundary nodes is slightly less than 2π due to the geometrical discretization error.

4.3. Solution accuracy

Next, we will study the convergence of the solution in the far field region. Fig. 4 plots the L^2-error of the radar cross section (RCS) as a function of the number of elements. The scatterer is a dielectric sphere of size $kr = 1$ and $\epsilon_r = 5$. We observe that the J- and D-VIE converge monotonically. In the case of the P-VIE, the convergence is not monotonic. The reason for this is not completely clear for us. The point-matching scheme may not be the best possible discretization procedure for this equation. Another problem may be the fact that the vector and scalar potentials are not properly coupled, i.e., the discrete basis function do not automatically satisfy the Lorentz gauge condition.

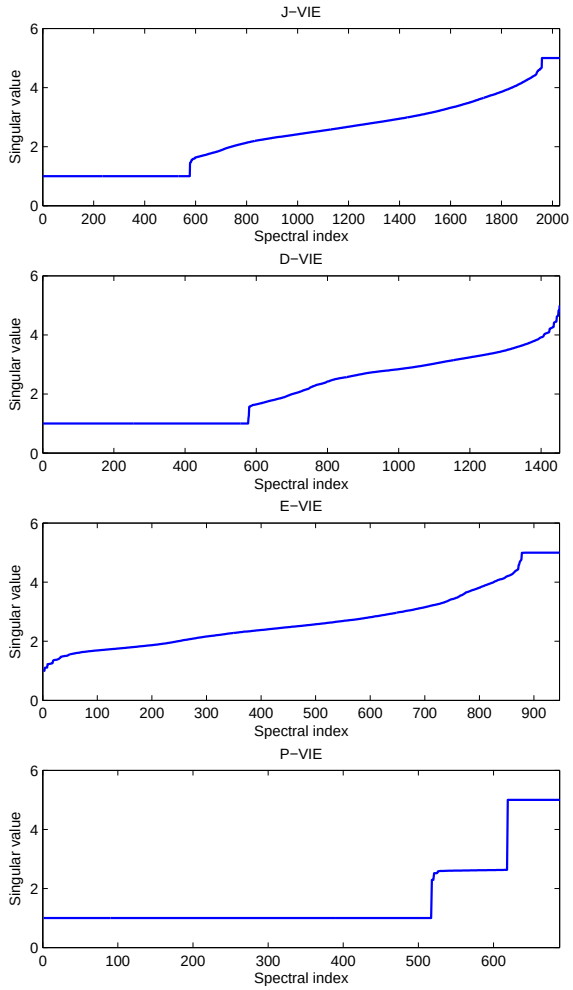

Figure 3: Real parts of eigenvalues with respect to spectral indices.

4.4. Discussion

Numerical results show that the discrete spectra of the analyzed volume-integral-equations depend on the permittivity. Particularly, the spectral radius increases with the permittivity which slows down the convergence of the iterative solver. It would be possible to implement a simple preconditioner for the potential formulation by scaling the scalar basis functions inside the object by ϵ_r and on the boundary by $(\epsilon_r + 1)/2$. This would result in eigenvalues clustering around a single point on the complex plane, and thus, would improve the convergence of the iterative solution. Similar preconditioner was proposed for the J-VIE in [16] but instead of scaling basis functions, finite-dimensional irrotational and harmonic subspaces needed to be scaled leading to a much more complicated preconditioner. Especially, building the discrete decomposition operators, required to separate the discrete subspaces, is a demanding task computationally. For the D- and E-VIE, similar decomposition operators are needed albeit for different function spaces.

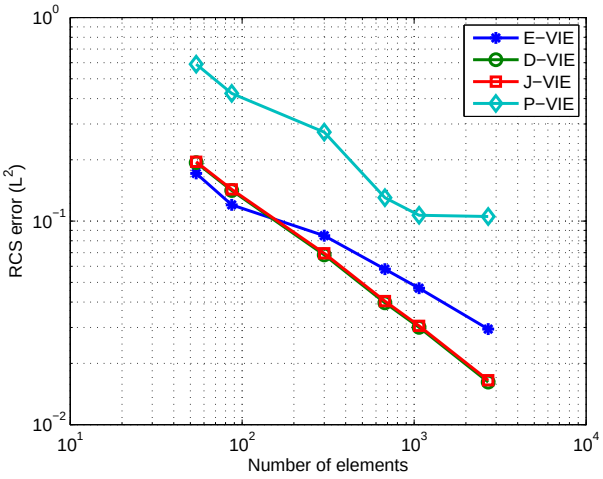

Figure 4: Relative error of the RCS a homogeneous sphere with $kr = 1$ and $\epsilon_r = 5$ as a function of the number of elements.

In addition, due to non-orthogonality of basis and testing functions, multiplication with the inverse of the Gram matrix may be required.

The drawback in the P-VIE is the poor accuracy of the solution when the equations are discretized with the nodal basis functions and the point matching on tetrahedral mesh. Using other discretization technique may improve the accuracy, but it may also affect the spectrum. For example, in [24] good accuracy was reported when the P-VIE was discretized with linear Lagrange interpolation nodal functions on curvilinear cubes and the point matching scheme. Hence, the P-VIE deserves to be studied in detail in the future.

5. Conclusions

We have studied spectral properties of the discretized counterparts of different volume-integral-equation formulations written for the current, flux density, field, and potentials as unknowns. The equations were discretized by standard techniques. The J-VIE formulations was discretized with piecewise constant, the D-VIE with the divergence conforming SWG, and the E-VIE with the curl conforming edge-elements as basis and testing functions. Continuous nodal scalar and vector functions were used as basis in the P-VIE together with the point-matching scheme. In the J-, D-, and E-formulations, the discrete spectrum (eigenvalue distribution) do not strictly follow the spectral theory of continuous operators. Thus, the discretized system may give rise to a spurious solution when an eigenvalue goes to zero. Particularly, this may happen when $\epsilon_r \leq 0$ [27]. In the D-VIE and E-VIE, the Gram matrix is not the identity matrix, hence, the discrete spectrum do not resemble the spectrum of the original operator. This effect, however can be removed by multiplying the discrete operator by the inverse of the Gram matrix.

The P-formulation is found to the be only formulation where the discrete spectrum follows the spectrum of the continuous operator. In the P-VIE, it is also straighforward to identify

the various parts of the spectrum on the complex plane. This property can be very useful from the preconditioning point of view. Particularly, by scaling the scalar potential basis functions associated to the interior and boundary nodes accordingly, the permittivity dependence can be removed from the discrete spectrum. This would accelerate the convergence of the iterative solution in case of high-contrast material which is a severe problem in the existing VIE and DDA implementations. On the other hand, the solution accuracy of the P-VIE is not as good as in the other considered formulations. This might be due to the fact that the applied point-matching technique does not satisfy the requirement of converging solutions, i.e., the integral operators are not tested in the dual of their range spaces. All of these properties, however, makes the P-formulation a very interesting topic of the future research.

Acknowledgment

The research has been funded by the ERC Advanced Grant No 320773 entitled "Scattering and Absorption of Electromagnetic Waves in Particulate Media" (SAEMPL).

[1] V. Rokhlin, Rapid solution of integral equations of classical potential theory, J. Computational Physics 60 (2) (1985) 187–207. doi:10.1016/0021-9991(85)90002-6.

[2] J. Goodman, P. Flatau, B. Draine, Application of fast-Fourier-transform techniques to the discrete-dipole approximation, Opt. Lett. 16 (15) (1991) 1198–1200. doi:10.1364/OL.16.001198.

[3] J. R. Phillips, J. K. White, A precorrected-FFT method for electrostatic analysis of complicated 3-D structures, IEEE Trans. CAD of Integ. Circ. and Sys. 16 (10) (1997) 1059–1072. doi:10.1109/43.662670.

[4] C.-C. Lu, A fast algorithm based on volume integral equation for analysis of arbitrarily shaped dielectric radomes, IEEE Trans. Ant. and Propag. 51 (3) (2003) 606–612. doi:10.1109/TAP.2003.809823.

[5] E. Bleszynski, M. Bleszynski, T. Jaroszewicz, AIM: Adaptive integral method for solving large-scale electromagnetic scattering and radiation problems, RADIO SCIENCE-WASHINGTON 31 (1996) 1225–1252.

[6] M. Yurkin, V. Maltsev, A. Hoekstra, The discrete dipole approximation for simulation of light scattering by particles much larger than the wavelength, J. Quant. Spectrosc. Radiat. Transfer 106 (2007) 546557. doi:10.1016/j.jqsrt.2007.01.033.

[7] M. Yurkin, D. De Kanter, A. Hoekstra, Accuracy of the discrete dipole approximation for simulation of optical properties of gold nanoparticles, Journal of Nanophotonics 4 (1) (2010) 041585–041585–15. doi:10.1117/1.3335329.

[8] J. Markkanen, C.-C. Lu, X. Cao, P. Yla-Oijala, Analysis of volume integral equation formulations for scattering by high-contrast penetrable objects, IEEE Trans. Ant. and Propag. 60 (5) (2012) 2367–2374. doi:10.1109/TAP.2012.2189704.

[9] M. Yurkin, Computational approaches for plasmonics, in: F. D. Sala, S. DAgostino (Eds.), Handbook of Molecular Plasmonics, Pan Stanford Publishing, 2013, pp. 83–135.

[10] N. V. Budko, A. B. Samokhin, Spectrum of the volume integral operator of electromagnetic scattering, SIAM Journal on Scientific Computing 28 (2) (2006) 682–700. doi:10.1137/050630660.

[11] M. Costabel, E. Darrigrand, E. Koné, Volume and surface integral equations for electromagnetic scattering by a dielectric body, Journal of Computational and Applied Mathematics 234 (6) (2010) 1817–1825. doi:10.1016/j.cam.2009.08.033.

[12] M. Costabel, E. Darrigrand, H. Sakly, The essential spectrum of the volume integral operator in electromagnetic scattering by a homogeneous body, Comptes Rendus Mathematique 350 (3) (2012) 193–197. doi:10.1016/j.crma.2012.01.017.

[13] J. Rahola, On the eigenvalues of the volume integral operator of electromagnetic scattering, SIAM Journal on Scientific Computing 21 (5) (2000) 1740–1754. doi:10.1137/S1064827598338962.

[14] M. A. Yurkin, M. Min, A. G. Hoekstra, Application of the discrete dipole approximation to very large refractive indices: Filtered coupled dipoles revived, Physical Review E 82 (3) (2010) 036703. doi:10.1103/PhysRevE.82.036703.

[15] D. Smunev, P. Chaumet, M. Yurkin, Rectangular dipoles in the discrete dipole approximation, J. Quant. Spectrosc. Radiat. Transfer 156 (2015) 67–79. doi:10.1016/j.jqsrt.2015.01.019.

[16] J. Markkanen, Discrete Helmholtz decomposition for electric current volume integral equation formulation, IEEE Trans. Ant. and Propag., 62 (12) (2014) 6282–6289. doi:10.1109/TAP.2014.2364614.

[17] D. Schaubert, D. Wilton, A. Glisson, A tetrahedral modeling method for electromagnetic scattering by arbitrarily inhomogeneous dielectric bodies, IEEE Trans. Ant. and Propag. 32 (1) (1984) 77–85. doi:10.1109/TAP.1984.1143193.

[18] C.-C. Lu, P. Ylä-Oijala, M. Taskinen, J. Sarvas, Comparison of two volume integral equation formulations for solving electromagnetic scattering by inhomogeneous dielectric objects, International IEEE AP-S Symposium 2009, Charleston, USA.

[19] L. Sun, W. Chew, A novel formulation of the volume integral equation for electromagnetic scattering, Waves in Random and Complex Media 19 (1) (2009) 162–180. doi:10.1080/17455030802545658.

[20] J. Markkanen, P. Ylä-Oijala, A. Sihvola, Discretization of volume integral equation formulations for extremely anisotropic materials, IEEE Trans. Ant. and Propag. 60 (11) (2012) 5195–5202. doi:10.1109/TAP.2012.2207675.

[21] P. De Doncker, A volume/surface potential formulation of the method of moments applied to electromagnetic scattering, Engineering analysis with boundary elements 27 (4) (2003) 325–331. doi:10.1016/S0955-7997(02)00120-0.

[22] W. Chew, E. Michielssen, J. M. Song, J. M. Jin (Eds.), Fast and Efficient Algorithms in Computational Electromagnetics, Artech House, Inc., Norwood, MA, USA, 2001.

[23] M. Li, W. C. Chew, Applying divergence-free condition in solving the volume integral equation, Progress In Electromagnetics Research 57 (2006) 311–333. doi:10.2528/PIER05061303.

[24] P. De Doncker, A potential integral equations method for electromagnetic scattering by penetrable bodies, IEEE Trans. Ant. and Propag., 49 (7) (2001) 1037–1042. doi:10.1109/8.933483.

[25] M. C. van Beurden, S. J. L. van Eijndhoven, Gaps in present discretization schemes for domain integral equations, International Conference on Electromagnetics in Advanced Applications, ICEAA 2007, Torino.

[26] M. C. van Beurden, S. J. L. van Eijndhoven, Well-posedness of domain integral equations for a dielectric object in homogeneous background, J. Eng. Math(2008) 62 (2008) 289–302. doi:10.1007/s10665-008-9218-2.

[27] O. Vartia, P. Ylä-Oijala, J. Markkanen, S. Puupponen, A. Seppälä, A. Sihvola, T. Ala-Nissila, On the applicability of discrete dipole approximation for plasmonic particles, J. Quant. Spectrosc. Radiat. Transfer 169 (2016) 2335. doi:10.1016/j.jqsrt.2015.10.003.